Differential sorting behavior for soluble and transmembrane cargoes at the *trans*-Golgi network in endocrine cells

Blake H. Hummer[a,†], Drew Maslar[a,†], Margarita Soltero-Gutierrez[a], Noah F. de Leeuw[b], and Cedric S. Asensio[a,*]

[a]Department of Biological Sciences and [b]Department of Physics and Astronomy, University of Denver, Denver, CO 80210

ABSTRACT **Regulated secretion of neuropeptides and peptide hormones by secretory granules (SGs) is central to physiology. Formation of SGs occurs at the *trans*-Golgi network (TGN) where their soluble cargo aggregates to form a dense core, but the mechanisms controlling the sorting of regulated secretory cargoes (soluble and transmembrane) away from constitutively secreted proteins remain unclear. Optimizing the use of the retention using selective hooks method in (neuro-)endocrine cells, we now quantify TGN budding kinetics of constitutive and regulated secretory cargoes. We further show that, by monitoring two cargoes simultaneously, it becomes possible to visualize sorting to the constitutive and regulated secretory pathways in real time. Further analysis of the localization of SG cargoes immediately after budding from the TGN revealed that, surprisingly, the bulk of two studied transmembrane SG cargoes (phogrin and VMAT2) does not sort directly onto SGs during budding, but rather exit the TGN into nonregulated vesicles to get incorporated to SGs at a later step. This differential behavior of soluble and transmembrane cargoes suggests a more complex model of SG biogenesis than anticipated.**

Monitoring Editor
Thomas Martin
University of Wisconsin, Madison

Received: Oct 8, 2019
Revised: Nov 26, 2019
Accepted: Dec 6, 2019

INTRODUCTION

Secretion of neuropeptides and peptide hormones such as insulin depends on their efficient sorting into secretory granules (SGs) that are capable of regulated exocytosis in response to an extracellular, physiological stimulus. Disturbances in their secretion underlie the development of pathological states such as type II diabetes. SGs bud from the *trans*-Golgi network (TGN) where their soluble cargoes aggregate to form a dense core (Tooze, 1998; Borgonovo *et al.*, 2006; Hou *et al.*, 2009; Park *et al.*, 2009). Two mechanisms have been proposed for sorting to SGs (Arvan and Halban, 2004). In the sorting by retention model, interactions in the lumen of the TGN drive the formation of SGs. Consistent with this, SGs contain large amounts of granulogenic proteins such as chromogranins that aggregate under the specific pH and redox conditions of the TGN. In this model, sorting to SGs thus occurs by default, with proteins destined for other organelles being removed from nascent SGs after budding from the TGN. This maturation can last up to several hours after budding and depends on clathrin as well as the adaptor protein AP-1 (Dittie *et al.*, 1996, 1997), but the functional significance of this process remains unclear and is likely to differ between specialized secretory cells. In contrast, the sorting for entry model involves active sorting of proteins destined for SGs at the TGN. In support of this model, biochemical analysis of budding from the TGN has demonstrated specific sorting of soluble proteins into SGs (Tooze and Huttner, 1990).

In addition to soluble cargoes, the membrane of SGs also contains several transmembrane proteins, and many of them such as the enzyme peptidylglycine α-amidating monooxygenase and the endothelial adhesion molecule P-selectin depend on cytosolic

This article was published online ahead of print in MBoC in Press (http://www.molbiolcell.org/cgi/doi/10.1091/mbc.E19-10-0561) on December 11, 2019.

†These authors contributed equally.

*Address correspondence to: Cedric S. Asensio (Cedric.Asensio@du.edu).

Abbreviations used: MCC, Manders correlation coefficient; NPY, neuropeptide Y; PBS, phosphate-buffered saline; ROI, region of interest; RUSH, retention using selective hook; SBP, streptavidin-binding peptide; SG, secretory granule; SgII, secretogranin II; TGN, *trans*-Golgi network; VMAT2, vesicular monoamine transporter.

sequences for their sorting to SGs (Milgram *et al.*, 1996; Blagoveshchenskaya *et al.*, 1999; El Meskini *et al.*, 2001). The neuronal vesicular monoamine transporter (VMAT2) fills secretory vesicles with monoamine neurotransmitters for exocytotic release and localizes preferentially to SGs in rat neuroendocrine PC12 cells (Liu *et al.*, 1994; Weihe *et al.*, 1994). The sorting of VMAT2 to SGs depends on a C-terminal cytoplasmic di-leucine-like motif with upstream acidic residues. Mutation of this motif diverts VMAT2 from the regulated to the constitutive secretory pathway, suggesting that these residues act as a sorting motif for the regulated secretory pathway (Krantz *et al.*, 2000; Li *et al.*, 2005). In addition, the other SG membrane proteins IA-2 and phogrin contain a similar sorting sequence, and phogrin also depends on this motif for sorting to the regulated secretory pathway in insulin-secreting cells (Torii *et al.*, 2005). However, the complete mechanisms contributing to sorting to SGs and indeed SG production remain poorly understood.

One of the main limitations to addressing this problem comes from the lack of sensitive approaches to evaluate sorting into pathways originating at the TGN. In the past, an elegant budding assay that relies on protein sulfation at the TGN has been used to demonstrate the specific sorting of proteins into nascent SGs (Tooze and Huttner, 1990). However, this assay is limited to the analysis of soluble SG cargo proteins that are both highly abundant and sulfated. It has therefore not been possible to monitor emergence from the TGN of lower abundance proteins, in particular integral membrane proteins, that are presumably not sulfated.

Here we report the optimization of the retention using selective hook (RUSH) system (Boncompain *et al.*, 2012) to visualize SG formation from (neuro-)endocrine cells and to obtain quantitative measurements of TGN budding of SG and non-SG soluble and transmembrane cargoes. We further monitor two cargoes simultaneously to visualize sorting to the constitutive and regulated secretory pathways in real time. We demonstrate that the transmembrane SG markers phogrin and VMAT2 do not localize with insulin directly after leaving the TGN but rather get added to SGs after budding.

RESULTS AND DISCUSSION

Visualization of SG formation using RUSH

To synchronize and visualize the movement of cargoes along the secretory pathway in (neuro-)endocrine cells, we used the RUSH system (Boncompain *et al.*, 2012). This approach relies on the compartmentalized expression of streptavidin acting as a "hook" for a coexpressed cargo fused to streptavidin-binding peptide (SBP). Exposure of cells to biotin leads to the rapid, synchronized release of the hooked cargoes. By using fluorescently tagged reporters, it becomes possible to follow a wave of cargo as it traffics through the secretory pathway. To test whether this approach could be applied to study the formation of SGs from (neuro-)endocrine cells, we began by determining the behavior of soluble SG cargoes. For this, we relied on neuropeptide Y (NPY) and secretogranin II (SgII) as their respective fusion to emdGFP (or other fluorescent proteins) targets properly to SGs in various (neuro-)endocrine cells including INS-1 and PC12 cells that we are using for this study (Taraska *et al.*, 2003; Courel *et al.*, 2008; Gandasi *et al.*, 2015). We fused emdGFP-SBP to the C-terminus of NPY (Supplemental Figure S1A) and transfected INS-1 and PC12 cells with optimized hook and cargo (NPY-emdGFP-SBP) plasmids together with a TGN marker (sialyltransferase-TagRFP657). As a first step, we validated that our cargo trafficked properly through the secretory pathway. In the absence of biotin, the reporter was found diffused across the cell, consistent with an ER localization, and treatment of cells with biotin led to its redistribution as expected. At 30 min, we observed strong localization at the TGN and following that time point the majority of the signal could be found in post-TGN vesicular carriers (Figure 1A; Supplemental Figure S1B). After 1 h of biotin treatment, NPY-emdGFP-SBP accumulated in discrete punctate structures that colocalized with endogenous insulin in INS-1 cells or endogenous SgII in PC12 cells (Figure 1B and Figure 3, B and D, later in the article; Supplemental Figure S1C). Similarly, SgII-emdGFP-SBP (Supplemental Figure S1A) colocalized with insulin in INS-1 cells (Figure 3G). We also determined the steady-state distribution of the reporters after incubating our cells with biotin for 24 h. NPY-emdGFP-SBP accumulated in SGs found at the tip of processes and colocalized with endogenous insulin (for INS-1 cells) or endogenous SgII (for PC12 cells). We also confirmed that NPY-emdGFP-SBP expressed as a full-length protein in both INS-1 and PC12 cells by Western blot and found lower molecular bands in INS-1 cells indicative of processing (Supplemental Figure S1D). These data suggest that these professional secretory cells are able to sort cargoes efficiently even under artificial conditions leading to a large wave of cargoes.

The ability to store SG cargo and release it under stimulatory conditions is a defining feature of (neuro-)endocrine cells. To further assess the functionality of our cargoes, we performed a secretion assay following RUSH. Working with INS-1 cells at first, we tested whether we could stimulate the release of NPY-emdGFP-SBP from newly formed SGs. Although we did not observe significant stimulation at 1.5 h postbiotin (Figure 1C), the amount of NPY-emdGFP-SBP secreted in response to depolarization (high K+) more than doubled at 3 h postbiotin (Figure 1D). We next performed experiments in PC12 cells and found that, under basal conditions, these cells secreted ~5% of total NPY-emdGFP-SBP; depolarization stimulated the release of NPY-emdGFP-SBP (~9-fold) at 1.5 h postbiotin (Figure 1E). Altogether these data suggest that our cargoes sort efficiently to the regulated secretory pathway. The data also indicate that SGs from PC12 cells become competent for regulated release faster than insulin SGs from INS-1 cells.

Determination of soluble and transmembrane SG cargo TGN budding kinetics

To visualize cargo movement along the secretory pathway, we imaged INS-1 cells expressing NPY-emdGFP-SBP or SgII-emdGFP-SBP live following the addition of biotin and observed a wave of fluorescent cargo entering the TGN labeled with sialyltransferase-TagRFP657. After reaching a peak, TGN fluorescence decreased concomitantly with the formation of post-TGN carriers (Supplemental Movie S1). We determined the ER exit rate constant (k_{ER}) by measuring the fluorescence change within the ER and fitting the data to a first-order decay curve. Next, we monitored the decrease in fluorescence at the TGN and fitted the data to extrapolate the TGN exit rate constant (k_{TGN}). Both constructs exited the ER at similar rates but NPY-emdGFP-SBP exited the TGN slightly faster than SgII-emdGFP-SBP (Figure 2). These data suggest that the trafficking rate through different organelles varies between cargoes. Consistent with this idea, the regulated secretory cargoes amylase and chymotrypsinogen undergo their main concentration between the ER and the *cis*-Golgi in pancreatic exocrine cells as opposed to the TGN (Oprins *et al.*, 2001). In the future, it will be interesting to compare the behavior of a variety of regulated secretory cargoes in different (neuro-)endocrine cells.

Next, we tested whether RUSH could be applied to study budding kinetics of SG transmembrane protein cargoes. For this, we relied on phogrin and VMAT2 (Supplemental Figure S1A), which both target efficiently to SGs in both INS-1 and PC12 cells (Liu *et al.*, 1994; Tsuboi *et al.*, 2000, Taraska *et al.*, 2003, Asensio *et al.*, 2010).

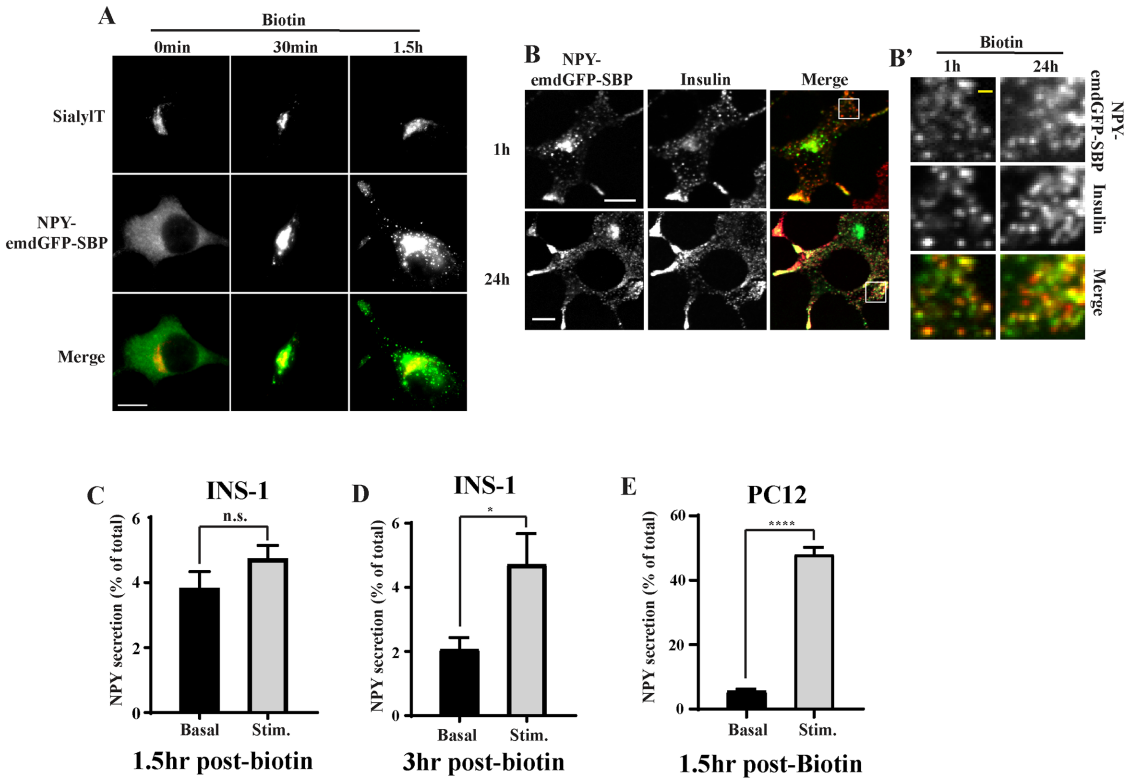

FIGURE 1: (A) INS-1 cells were transfected with NPY-emdGFP-SBP together with the TGN marker sialyltransferase-TagRFP657 and ER-hook, incubated with biotin for the indicated times, fixed, and imaged using a widefield epifluorescence microscope. (B) INS-1 cells transfected with RUSH constructs were incubated with biotin for 1 or 24 h, fixed, and immunostained for insulin followed by Alexa Fluor 647–conjugated secondary antibodies. Cells were imaged by spinning-disk confocal microscopy. Insets denoted by a square are shown in B′. INS-1 (C, D) or PC12 cells (E) were transfected with NPY-emdGFP-SBP and ER hook for secretion assays. Cells were incubated with biotin for 1.5 h (C, E) or 3 h (D) followed by exposure to basal or stimulated conditions for 15 min. Secretion was determined by reading the fluorescence in the media and was normalized to total fluorescence in cell lysate. *$p < 0.05$, ****$p < 0.0001$ relative to NPY basal (for INS-1 cells 1.5 h, $n = 3$, for INS-1 cells 3 h, $n = 4$, for PC12 cells $n = 3$) by unpaired two-tailed t test. Data shown indicate mean ± SEM. Scale bar indicates 10 μm and 1 μm for insets.

By Western blot, we found that phogrin-emdGFP-SBP expressed as a full-length protein in both INS-1 and PC12 cells and observed lower molecular bands in INS-1 cells indicative of processing (Supplemental Figure S1D). In the absence of biotin, phogrin-emdGFP-SBP was found diffused across the cell, consistent with an ER localization, and treatment of cells with biotin led to its redistribution as expected. At 40 min, we observed strong localization at the TGN and following that time point the majority of the signal could be found in post-TGN vesicular carriers (Supplemental Figure S2A). Live imaging experiments in INS-1 cells revealed that phogrin-emdGFP-SBP and VMAT2-emdGFP-SBP exited the ER with similar kinetics, which were slower than the ones measured for soluble regulated SG cargoes. Phogrin-emdGFP-SBP exited the TGN with similar kinetics than SgII-emdGFP-SBP, and VMAT2-emdGFP-SBP budding rate was significantly slower (Figure 2; Supplemental Movie S1). Importantly, our imaging conditions led to minimal photobleaching (Supplemental Figure S2, B and C). Our data illustrate that secretory cargoes exit the TGN at specific rates with soluble SG cargoes tending to traffic faster than transmembrane SG cargoes. Intuitively, this seems logical as the relative enrichment of soluble versus transmembrane proteins on SGs is biased toward soluble cargoes by at least one or two orders of magnitude (Suckale and Solimena, 2010). It is also possible that these cargoes get modified to various extents as they traffic through the secretory pathway and that these protein modification steps contribute to the difference in kinetics.

Transmembrane SG cargoes do not exit the TGN within SGs but get recruited later

Surprisingly, when looking at phogrin-emdGFP-SBP and VMAT2-emdGFP-SBP localization after 1 h of biotin, we found that they did not colocalize with insulin unlike NPY-emdGFP-SBP and SgII-emdGFP-SBP (Figure 3). However, we observed robust accumulation at the tip of processes after 24 h of biotin treatment, suggesting that these fusion proteins eventually traffic properly (Figure 3). Time course experiments revealed that the enrichment within insulin granules increases gradually to peak at around 8 h postbiotin (Supplemental Figure S2D). In addition, we obtained similar results after pulsing our cells with biotin for 30 min followed by extensive washes to enable hooking of cargo synthesized after the initial wave (Supplemental Figure S2E). This indicates that continuous synthesis of cargo happening after the initial release of the hooked cargo is not responsible for the increase in colocalization observed at later time points. These data suggest that, at least using this approach, phogrin-emdGFP-SBP and VMAT2-emdGFP-SBP might exit the TGN within nonregulated vesicles, likely constitutive secretory carriers, and get incorporated to SGs only later, possibly during SG maturation.

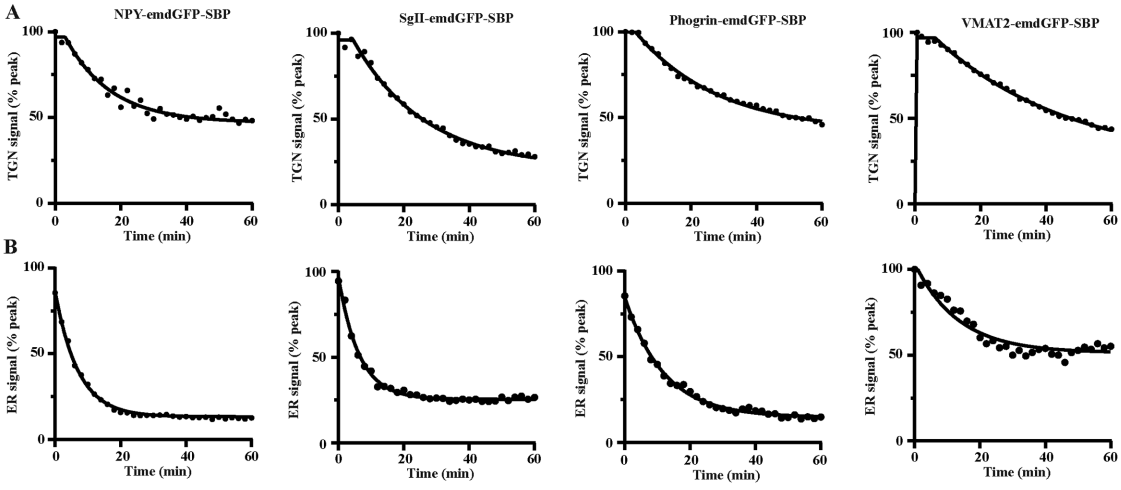

C

	$k_{TGN\ (min^{-1})} \pm SEM$	$k_{ER\ (min^{-1})} \pm SEM$
NPY-emdGFP-SBP	*0.073 ± 0.007*	*0.151 ± 0.012*
SgII-emdGFP-SBP	*0.045 ± 0.004*	*0.142 ± 0.012*
Phogrin--emdGFP-SBP	*0.042 ± 0.005*	*0.086 ± 0.007*
VMAT2--emdGFP-SBP	*0.027 ± 0.004*	*0.080 ± 0.015*

FIGURE 2: INS-1 cells were transfected as in Figure 1 with the indicated cargoes. Fluorescence within the TGN region (A) and the ER (B) was monitored and the data were fitted using a first-order kinetic model to extrapolate ER (k_{ER}) and TGN rate constants (C). Representative curves are shown for each cargo ($n = 16$ for NPY-emdGFP-SBP from three independent transfections; $n = 8$ for SgII-emdGFP-SBP from two independent transfections; $n = 14$ for phogrin-emdGFP-SBP from three independent transfections; $n = 11$ for VMAT2-emdGFP-SBP from two independent transfections).

To test this hypothesis more directly, we repeated the experiments in the presence of the dynamin inhibitor dynasore in INS-1 cells. Dynamin II mediates the scission of constitutive secretory vesicles at the TGN (Jones *et al.*, 1998; Kockx *et al.*, 2014). As a positive control, we looked at the behavior of a bona fide transmembrane marker of constitutive secretory vesicles, SBP-emdGFP-VSV-G (Supplemental Figure S1A) (Rivas and Moore, 1989). We first validated that SBP-emdGFP-VSV-G trafficked properly through the secretory pathway (Figure 3B; Supplemental Movie S1). Indeed, after 1 h of biotin, we could observe accumulation of this marker at the plasma membrane as expected, suggesting that it is reaching the cell surface in a constitutive manner and it did not colocalize with insulin at 1 or 24 h (Figure 3, B–D). Dynasore treatment led to the accumulation of SBP-emdGFP-VSV-G in the TGN region and slowed down its budding kinetics (Figure 4, A and B). As a consequence, we could not detect post-TGN carriers in cells treated with dynasore postpeak, whereas they were readily detectable in vehicle-treated cells (Figure 4A′, arrows). In contrast, dynasore treatment slowed down budding of NPY-emdGFP-SBP to a lesser extent (Figure 4, C and D). As a consequence, we could still observe budded SGs in the presence of the inhibitor (Figure 4C′). Next, we performed the same experiments with phogrin-emdGFP-SBP and VMAT2-emdGFP-SBP and observed that dynasore treatment prevented budding from the TGN of both cargoes (Figure 4, E and F; Supplemental Figure S2F). These data suggest that transmembrane SG cargoes exit the TGN within nonregulated secretory vesicles.

Simultaneous visualization of constitutive and regulated secretory cargo budding from TGN

To further distinguish sorting of cargoes to the constitutive and regulated secretory pathways, we next tested whether we could follow two cargoes simultaneously. For this, we generated NPY-mCherry-SBP that we coexpressed with SgII-emdGFP-SBP, phogrin-emdGFP-SBP, or SBP-emdGFP-VSV-G. To visualize budding from the TGN, we imaged our cells after 40 min of biotin treatment in order to get a wave of cargoes to the TGN. To our knowledge, this represents the first successful attempt at simultaneously imaging cargo sorting to constitutive versus regulated secretory pathways in real time. When looking at two soluble regulated secretory cargoes, the majority of budding vesicles contained both NPY-mCherry-SBP and SgII-emdGFP-SBP (Figure 5, A–C; Supplemental Movie S2). On the other hand, we observed significantly less NPY-mCherry-SBP vesicles being positive for SBP-emdGFP-VSV-G (Figure 5, B and C; Supplemental Movie S2), as expected for two cargoes known to traffic to the regulated and constitutive secretory pathway, respectively. Interestingly, the proportion of NPY-mCherry-SBP vesicles also positive for phogrin-emdGFP-SBP was similar to SBP-emdGFP-VSV-G (Figure 5, B and C; Supplemental Movie S2), indicating again that phogrin exits the TGN within nonregulated secretory vesicles.

Finally, we repeated the same experiment in presence of dynasore to block or slow down vesicle budding from the TGN. The treatment impeded vesicular movement of all studied cargoes (Supplemental Movie S2), but the effect seemed more pronounced for SBP-emdGFP-VSV-G and phogrin-emdGFP-SBP, resulting in a more arrested distribution around the Golgi area. NPY-mCherry-SBP did not colocalize with these arrested vesicles, whereas it did colocalize with SgII-emdGFP-SBP (Figure 5, D–G). Additionally, these soluble regulated secretory cargoes seemed more dynamic. Altogether these results indicate that phogrin-emdGFP-SBP do not exit the Golgi within vesicles containing soluble regulated secretory cargoes and suggests that it gets added to SGs postbudding. Interestingly, analysis of phogrin recycling after exocytosis has revealed that it can reach an insulin-positive compartment from the plasma membrane without first recycling back to the TGN (Vo *et al.*, 2004). Consistent

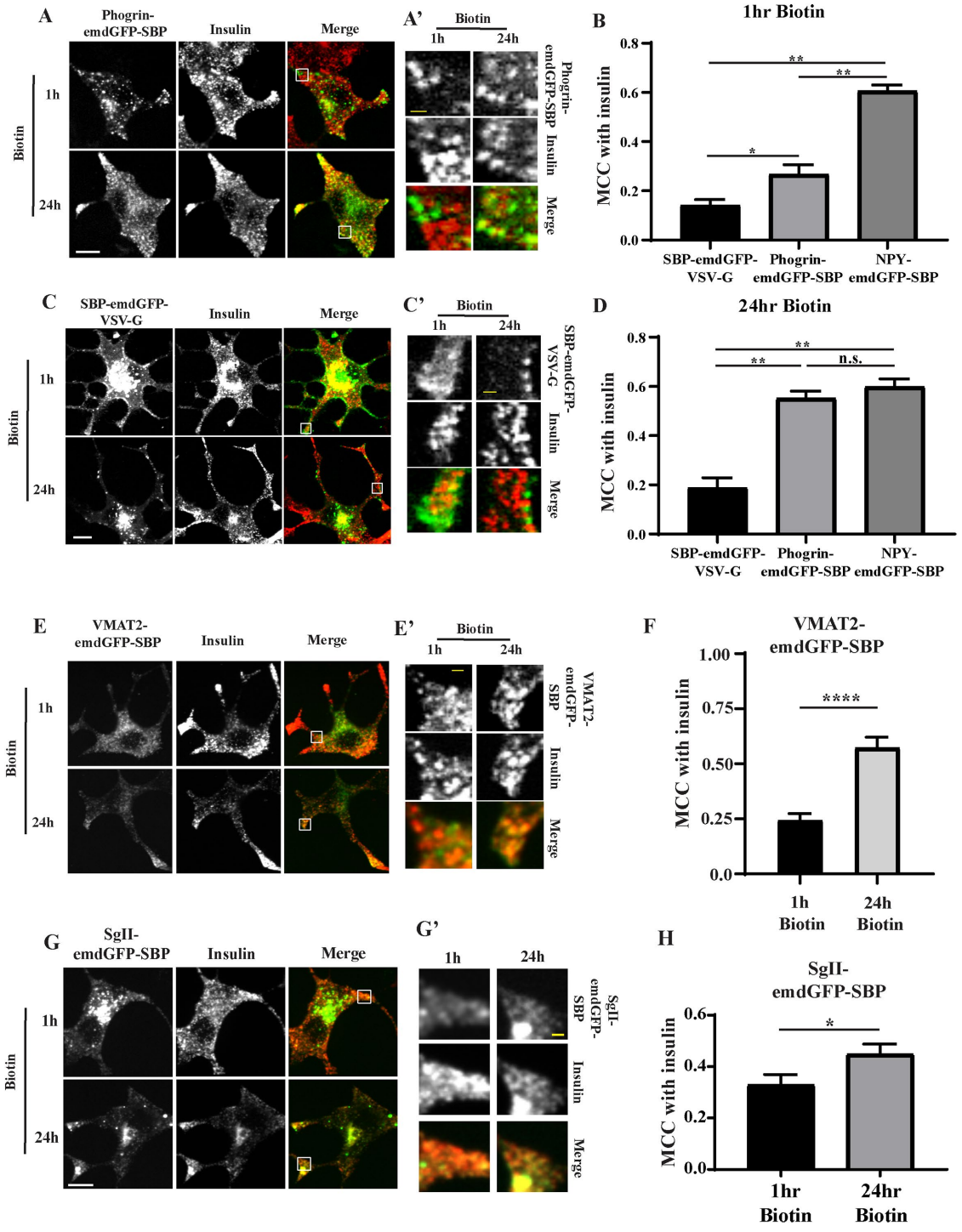

FIGURE 3: INS-1 cells were transfected with phogrin-emdGFP-SBP (A) or SBP-emdGFP-VSV-G (B) and incubated with biotin as in Figure 1. (A) INS-1 cells were costained for insulin at 1 or 24 h. Insets denoted by a square are shown in A′ and C′. The extent of colocalization with insulin was determined by MCC at 1 h (B) and 24 h (D). MCC was also calculated for NPY-emdGFP-SBP for comparison using the images shown in Figure 1; *$p < 0.05$; **$p < 0.01$ by one-way ANOVA followed by posthoc Tukey *t* test (for SBP-emdGFP-VSV-G 1 h biotin, $n = 21$ cells from two independent transfections; for SBP-emdGFP-VSV-G 24 h biotin, $n = 28$ from three independent transfections; for phogrin-emdGFP-SBP 1 h biotin, $n = 21$ cells from two independent transfections; for phogrin-emdGFP-SBP 24 h biotin, $n = 28$ from three independent transfections; for NPY-emdGFP-SBP 1 h biotin, $n = 26$ cells; for NPY-emdGFP-SBP 24 h biotin, $n = 29$ cells). (E–H) INS-1 cells were transfected with VMAT2-emdGFP-SBP (E) or SgII-emdGFP-SBP (G) and costained for insulin at 1 or 24 h. Insets denoted by a square are shown in E′ and G′. The extent of colocalization with insulin was determined by MCC at 1 and 24 h for VMAT2-emdGFP-SBP (F) and SgII-emdGFP-SBP (G); *$p < 0.05$, ****$p < 0.0001$ by unpaired *t* test (for VMAT2-emdGFP-VSV-G 1 h biotin, $n = 21$ cells; for 24 h biotin, $n = 12$ cells from two independent transfections; for SgII-emdGFP-SBP 1 h biotin, $n = 24$ cells; for 24 h biotin, $n = 22$ cells from three independent transfections). Data shown indicate mean ± SEM. Scale bar indicates 10 μm and 1 μm for insets.

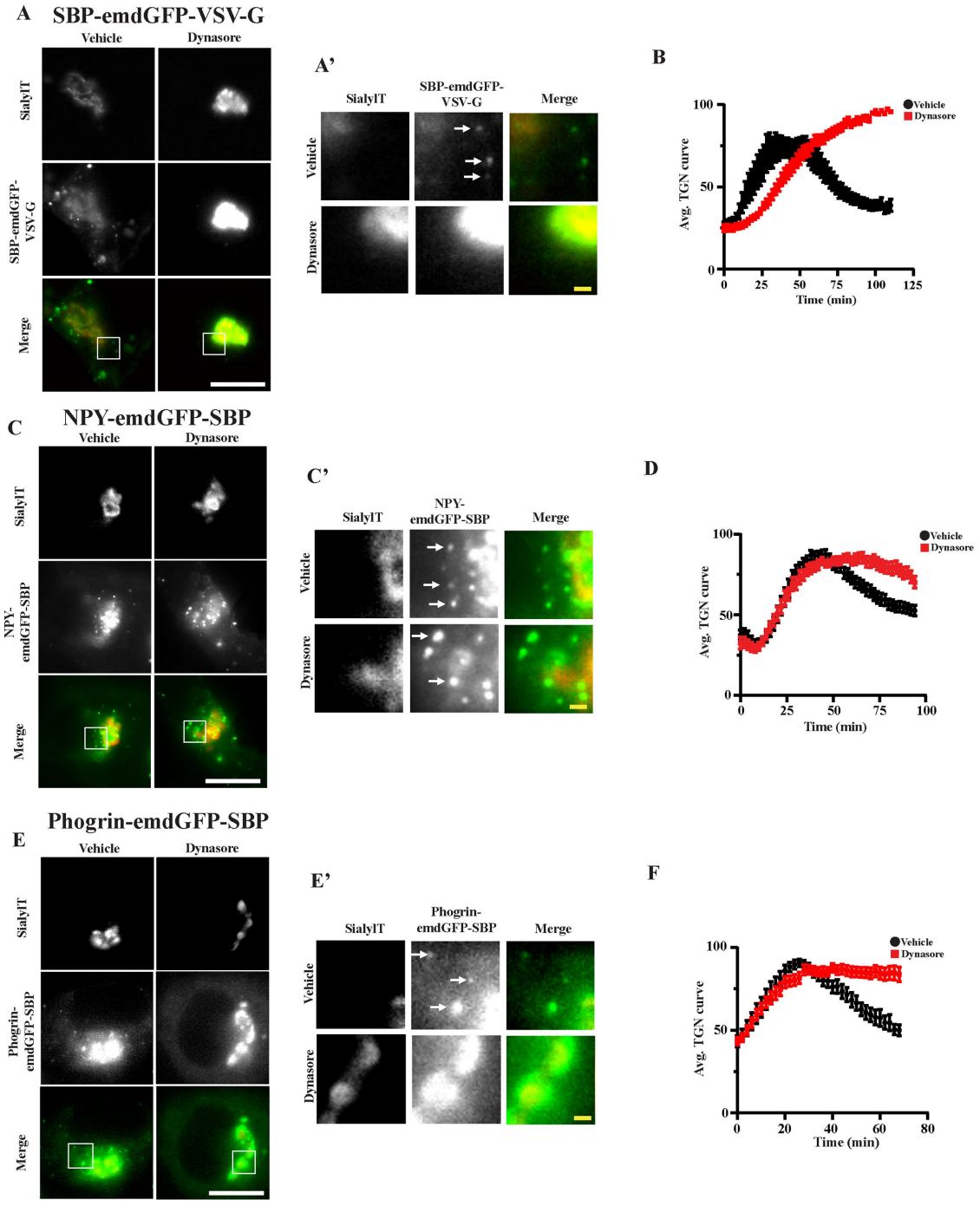

FIGURE 4: INS-1 cells transfected with the indicated cargoes were incubated with biotin in presence or absence of 80 μM dynasore. Fluorescence within the TGN region was monitored as described in Figure 2A. Insets are shown in A′, C′, and E′. Arrows indicate post-TGN carriers. Average curves of TGN fluorescence are shown in B, D, and F ($n = 9$ and 9 cells from two independent transfections for SBP-emdGFP-VSV-G vehicle and dynasore, respectively; $n = 19$ and 20 cells from independent transfections for NPY-emdGFP-SBP vehicle and dynasore, respectively; $n = 7$ and 12 cells from three independent transfections for phogrin-emdGFP-SBP vehicle and dynasore, respectively). Data shown indicate mean ± SEM. Scale bar indicates 10 μm and 1 μm for insets.

with this idea, several genes typically associated with the endocytic and retrograde pathways affect SG formation (Asensio *et al.*, 2010, 2013; Sasidharan *et al.*, 2012; Sirkis *et al.*, 2013; Paquin *et al.*, 2016; Topalidou *et al.*, 2016; Zhang *et al.*, 2017).

This leaves the question as to how transmembrane cargoes meant for SGs initially leave the Golgi and end up on SGs. We propose a model in which transmembrane cargoes are initially sorted to unregulated vesicles that fuse with the plasma membrane. Following recycling of the cargo protein (i.e., phogrin, VMAT2) from the plasma membrane, they are then properly added to immature SGs, presumably from endosomal compartments. This suggests that a fusion step between endosomal-derived vesicles and immature SGs occurs during maturation. We have not been able to observe fusion events between vesicles containing a transmembrane SG cargo and

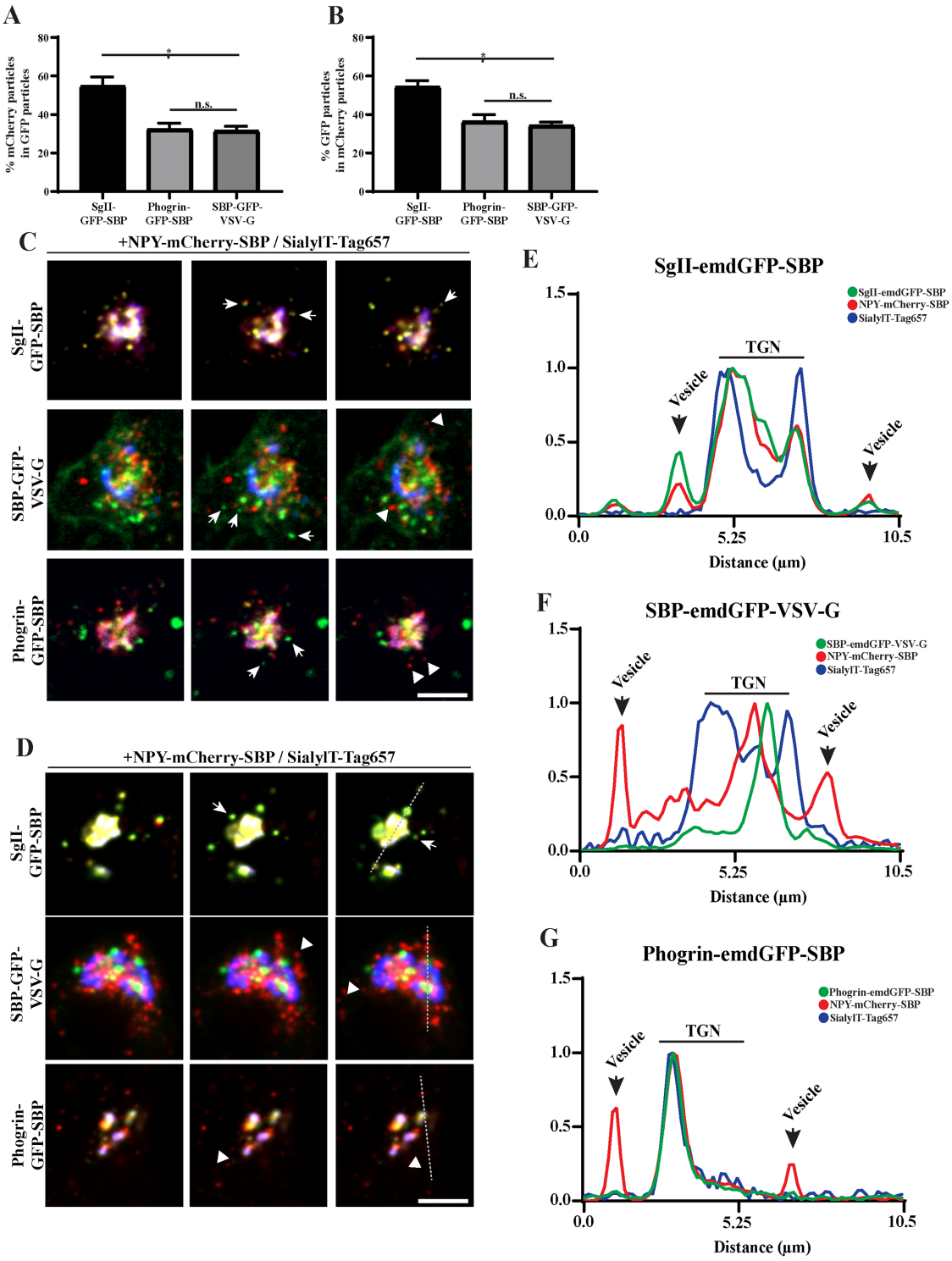

FIGURE 5: (A–C) INS-1 cells cotransfected with NPY-mCherry-SBP and indicated emdGFP-RUSH constructs as in Figure 2 and imaged every 300 ms for 2 min after 40 min of biotin treatment. The proportion of vesicles positive for both markers was determined (A, B); *$p < 0.0001$ ($n = 14$ cells for SgII-emdGFP-SBP; $n = 12$ for phogrin-emdGFP-SBP; $n = 19$ for SBP-emdGFP-VSV-G from two independent transfections) by one-way ANOVA followed by post hoc Tukey t test. Data shown indicate mean ± SEM. Consecutive frames from the movies are shown in C. (D–G) INS-1 cells cotransfected with NPY-mCherry-SBP and indicated emdGFP-RUSH constructs as in Figure 2 and imaged every 300 ms for 2 min after 40 min of biotin and dynasore treatment. Consecutive frames from the movies are shown in D. (E–G) Line-scan profiles from a single frame from a single representative movie represent the fluorescence intensity across the TGN and its vicinity. Arrows indicate vesicles positive for both markers; arrowheads indicate vesicles positive for one marker. Scale bar indicates 10 µm.

soluble SG cargo under our fast imaging conditions. This is likely because we looked only at early postbiotin time points. By focusing on later time points, where colocalization is increased between transmembrane SG cargoes and endogenous insulin, we anticipate to observe such fusion events. It will be interesting to test this hypothesis in the future, as well as determining the exact step and molecular players controlling the recruitment of phogrin, and whether this mechanism holds true for all transmembrane SG cargoes. This will provide invaluable information about the mechanisms controlling sorting of transmembrane proteins.

MATERIAL AND METHODS

Molecular biology

The following primers were used for cloning. P1: 5′-ACCGGTCCACCATGTTAGGTAACAAGCG-3′; P2: 5′-CTTGCTCACAAGCTTCCACATTGCAGGG-3′; P3: 5′-ATGTGGAAGCTTGTGAGCAAGGGCGAGGA-3′; P4: 5′-TCTCCTGAACCTCCGAGCTCCTTGTACAGCTCGTCCATGC-3′; P5: 5′-GAGCTCGGAGGTTCAGGAGACGAGAAGACCACTGGTTG-3′; P6:5′- GAATTCTTATGGTTCACGTTGACCTTGTG-3′; P7: 5′-AGCTTTACCCATACGACGTACCAGATTACGCTGAGCT-3′; P8: 5′-CAGCGTAATCTGGTACGTCGTATGGGTAA-3′; P9: 5′-CCGTCAGATCCGCTAGCGCTACCGGTCCACCATGGGGCTACCGCTCCCG-3′; P10: 5′-CGCCCTTGCTCACTACCTTTCCTTTCGGCCTGATTCCA-3′; P11: 5′-AGGTAGTGAGCAAGGGCGAGGAGC-3′; P12: 5′-TAGGAGCTTGAGTCCTGGTTCACGTTGACCTTGTG-3′; P13: 5′-GAACCAGGACTCAAGCTCCTACCCCATCCAG-3′; P14: 5′-CCGTCAGATCCGCTAGCGCTACCGGTCCACCATGACTGAATCGAAGGCTTACC-3′; P15: 5′-AGCTCCTCGCCCTTGCTCACAAGCTTCATGTTTTCCATGGCCCGT-3′; P16: 5′-GGAGGAGGttcaGGAGAATTCaagttcaccatagtttttccac-3′; P17: 5′-GGATCCCGGGCCCGCGGTACCTTActttccaagtcggttcatc-3′; P18: 5′-ATAACCGGTAGCACTAGCGGCGGAAGCGGCGGGACAGGTGGAGTGAGCAAGGGCGAGGAG-3′; P19: 5′-ATAACCGGTGCCACCGGAGCCTCCGGTTCCGCCGCTGCCACCTGGTTCACGTTGACCTTG-3′; P20: 5′-ATATAAGCTTGTGAGCAAGGGCGAGGAG-3′; P21: 5′-ATATGAGCTCcttgtacagCTCGTCCATGCC-3′.

Previous studies utilizing RUSH performed the assay using a bicistronic plasmid containing an ER hook (KDEL-streptavidin) followed by a "hookable" cargo after an IRES (Boncompain *et al.*, 2012; Chen *et al.*, 2017; Emperador-Melero *et al.*, 2018). When these cargoes were tested in COS-7 cells, they behaved as expected (unpublished data), but they did not in (neuro-)endocrine cells. The fusion proteins expressed at very low levels and the cells did not display any RUSH on biotin addition. To alleviate this, we expressed the hook and cargo using two separate plasmids, which solved the issue of low expression; however, this alone did not allow for RUSH to occur due to cargo not being hooked properly. We further engineered our ER hook by introducing a linker between the streptavidin and the KDEL sequence. This modification was essential and sufficient to enable efficient hooking at the ER. All constructs used were generated using pemdGFPC3 as a backbone. STR-HA-KDEL: HA-KDEL was produced by annealing P19 and P20. The product was used in a ligation reaction with pemdGFPC3-STR cut with *Sbf*1 and *Sac*1. To generate STR-Linker-KDEL, we introduced a flexible linker by annealing P21 and P22 and ligating into STR-HA-KDEL cut with *Sbf*I and *Sac*I, which removed the HA. To generate NPY-emdGFP-SBP, we amplified NPY using P1 and P2, emdGFP using P3 and P4, and SBP using P5 and P6. We performed overlap extension PCR using emdGFP and SBP fragments. NPY, emdGFP-SBP, and pemdGFPC3 cut with *Age*I and *Eco*R1 were used in a three-part Gibson reaction. To generate NPY-HA-SBP, HA was obtained by annealing P7 and P8. The annealed primers were used in a ligation reaction with NPY-emdGFP-SBP cut with *Hin*dIII and *Sac*I, which removed emdGFP. To generate phogrin-emdGFP-SBP, phogrin's lumenal domain up to the transmembrane domain was amplified using P9 and P9. The emdGFP-SBP was amplified using P10 and P11. The remaining portion of phogrin's lumenal domain and the transmembrane plus cytosolic domain was amplified using P12 and P13. The emdGFP-SBP and cytosolic portion of phogrin underwent overlap extension. We introduced emdGFP-SBP within the lumenal domain (after amino acid 588). This construct was designed based on the extensive, unpublished work done in the laboratory of the late John Hutton (Barbara Davis Center for Childhood Diabetes, University of Colorado School of Medicine), where a pHluorin-phogrin fusion was generated (Bauer, 2008). This construct was validated by showing that, at this particular site, the insertion of the fluorescent protein did not affect the trafficking of phogrin in INS-1 cells. To generate SgII-emdGFP-SBP, *SgI*I was amplified using P14 and P15 and ligated pemdGFPC3-emdGFP-SBP cut with *Age*I and *Hin*dIII. To generate SBP-emdGFP-VSV-G, VSVG was amplified using P16 and P17. A vector containing SBP-emdGFP was cut with *Eco*RI and *Kpn*I. PCR and vector were used in a Gibson reaction to generate SBP-emdGFP-VSVG. To generate VMAT2-emdGFP-SBP, we inserted emdGFP-SBP within the first lumenal loop of VMAT2. Indeed, insertion of pHluorin at this particular site does not affect VMAT2's trafficking (Anantharam *et al.*, 2010). To amplify emdGFP-SBP, we used P18 and P19 and ligated into pemdGFPC3-VMAT2 cut with *Age*I. To generate NPY-mCherry-SBP, we amplified mCherry using P20 and P21 and ligated within NPY-emdGFP-SBP cut with *Hin*dIII and *Sac*I. All constructs were verified by Sanger sequencing (Quintarabio). Primers were obtained from IDT and restriction enzymes from NEB.

Antibodies

The following primary antibodies were used in this study: mouse anti-insulin (Assady *et al.*, 2001) (Sigma SAB4200691), dilution 1:1000; rabbit anti-SgII (Sirkis *et al.*, 2013) (Meridian K55101R), dilution 1:2000; rat anti-HA (Hummer *et al.*, 2017) (Sigma 12158167001), dilution 1:500. The following secondary antibodies were used: goat anti-mouse Alexa Fluor 647 (Invitrogen A32728), dilution 1:2000; goat anti-rabbit Alexa Fluor 647 (Invitrogen A21244), dilution 1:2000; goat anti-rat Alexa Fluor 647 (Invitrogen A21247), dilution 1:2000.

Cell culture and transfection

INS-1 cells (University of Michigan) were cultured in RPMI 1640 (Genesee Scientific, Cat# 25-506H) with 10% fetal bovine serum (VWR, Cat#89510-186) and 1 mM sodium pyruvate (Genesee Scientific, Cat#25-537) in 5% CO_2 at 37°C. PC12 cells (University of California, San Francisco) were cultured in DMEM (Genesee Scientific, Cat#25-501) with 10% horse serum and 5% cosmic calf serum in 5% CO_2 at 37°C. Transfections for live imaging were performed using Fugene HD (Promega, Cat#E2311) according to the manufacturer protocol. For RUSH, a ratio of 3:1 hook to cargo ratio was determined to be ideal. Lipofectamine 2000 was used to transfect PC12 cells for secretion assays. Experiments were performed 36–48 h after transfection. Cells were routinely tested for the absence of mycoplasma. For live imaging, cells were transfected in 24-well dishes (Genesee Scientific, Cat#25-107), trypsinized, and replated 24 h posttransfection to a 35-mm glass bottom imaging dish coated with PLL (Sigma-Aldrich, Cat#P2636). Cells were imaged the following day. For live imaging, INS-1 were transferred to biotin and phenol-red free RPMI (US Biological Life Sciences, Cat#R9002-01) media supplemented with 2.4 mM sodium bicarbonate and 25 mM HEPES. PC12 cells were imaged in phenol-red free complete media.

Immunofluorescence

Cells were fixed in 4% paraformaldehyde in phosphate-buffered saline (PBS) for 20 min, permeabilized with 0.1% Triton X-100 in PBS, incubated in PBS block buffer (2% bovine serum albumin, 1% fish skin gelatin, 0.02% Saponin) for 1 h, incubated with primary antibodies for 1 h, and followed by incubation with secondary antibodies for 1 h.

Secretion assays

PC12 or INS-1 cells were seeded onto a 24-well cell culture dish coated with or without PLL, respectively. INS-1 cells were washed once in PBS and reset in low potassium KRB (138 mM NaCl, 5.4 mM KCl, 2.6 mM $MgSO_4$, 5.0 mM $NaHCO_3$, 10 mM HEPES, 2.6 mM $CaCl_2$, 1.5 mM glucose) for 1 h at 37°C. Following an additional PBS wash, cells were incubated with low potassium KRB with 50 µM biotin (Sigma-Aldrich, Cat#B4501-1G) for 3 h. Cells were washed again with PBS and treated with low or high potassium (97.8 mM NaCl, 45.6 mM KCl) KRB for 15 min. Secreted fractions were collected. Cells were washed with ice-cold PBS and lysed in 50 mM Tris, pH 7.4, 150 mM NaCl, mM EDTA, 1% TX-100 with protease inhibitors (Sigma-Aldrich), and 1 mM phenylmethylsulfonyl fluoride (Sigma-Aldrich). Secreted fractions and cellular lysates were prepared and fluorescence was measured using a plate reader as described previously (Hummer *et al.*, 2017). PC12 cells were washed with PBS and incubated with complete media in the presence of 50 µM biotin for 1.5 h at 37°C. Following an additional PBS wash, cells were incubated with low or high potassium Tyrode buffer for 15 min at 37°C. Secreted and cellular fractions were prepared as described above.

Image acquisition and analysis

Images for colocalization analysis were acquired using a custom-built Nikon spinning disk confocal. Images were collected with a 63× objective (Oil Plan Apo NA 1.49) and an ImageEM X2 EM-CCD camera (Hamamatsu, Japan) at a resolution of 512 × 512 pixels. Images for puncta analysis were imaged on an Evos FL Auto 2 microscope using a 63× objective (Oil Plan Apo NA 1.42; Olympus). Manders correlation coefficient (MCC) was determined using the Colocalization Threshold Fiji plug-in using a region of interest (ROI) that encompassed the entire cell but excluded the nucleus and Golgi region. Cells were excluded from analysis for tM1 or tM2 values of 1 due to thresholding issues, and cells with no positive correlation were also excluded. Live movies were imaged on an Evos FL Auto 2 in an environmentally controlled imaging chamber (37°C, 5% CO_2, 20% humidity). Cells were imaged every 2 min. Image processing was performed using MATLAB software. To isolate ROIs, each frame of the Golgi-labeled channel was manually cropped around the general cell area and segmented using an intensity threshold filter. The segmented ROI was constrained by an area filter to reduce noise, generating a binary mask of only the largest objects within the frame. The mask was then convoluted with the cargo channel to obtain the TGN signal, and the inverse of the mask was convoluted with the same channel to acquire the background signal. For figures, images were processed using ImageJ; any changes in brightness and contrast were identical between samples meant for comparison. First-order decay curves were fitted using GraphPad Prism version 8.0.2 for Windows (GraphPad Software, La Jolla, CA). The plateau followed by a one-phase decay function with a constraint of X0 greater than 0 was used to fit k_{TGN}. The one-phase decay function was used to fit k_{ER}. Average curves for experiments with dynasore were made by combining the curves from all cells starting directly after biotin addition. For phogrin, due to variable RUSH starting time, we aligned the individual curves at the beginning of ER exit to generate average curves. Statistical analysis was performed using Prism. The following criteria were used to exclude cells from further analysis: 1) cell division, 2) excessive Golgi fractionation, or 3) extensive out of focus drift. Outside of these criteria, all cells were used for analysis. For two cargo RUSH experiments, transfected cells were imaged using a spinning-disk confocal 30–40 min after biotin addition every 300 ms for 2 min. We determined the proportion of newly budded vesicles containing both cargoes using the ComDet v.0.4.2 plug-in for ImageJ (https://github.com/ekatrukha/ComDet) using a circular ROI around the Golgi region with a diameter that equals to twice the diameter of the Golgi. Proportions were obtained for each frame, and an average proportion per cell was calculated over 150 frames. Line scans were generated using ImageJ by measuring fluorescence intensity from individual frames from a single movie. Raw fluorescence measurements were normalized to 1 for each fluorescent reporter included on the line scan. Representative movies were selected from a total of 11 movies for phogrin and VSV-G and 12 movies of SgII. All movies showed a similar effect in blockade of traffic for transmembrane cargoes with little perturbation of soluble cargoes following dynasore treatment.

ACKNOWLEDGMENTS

We thank Peter Arvan for the INS-1 cell line and Dinah Loerke for help with image analysis; Str-KDEL ManII-SBP-EGFP was a gift from Franck Perez (Addgene plasmid # 65252; http://n2t.net/addgene:65252; RRID:Addgene_65252). This work was supported by American Diabetes Association Grant #1-17-JDF-064 and by National Institute of General Medical Sciences Grants R01 GM124035 and R15 GM116096 to C.S.A. We thank Katharine Roth for technical support.

REFERENCES

Anantharam A, Onoa B, Edwards RH, Holz RW, Axelrod D (2010). Localized topological changes of the plasma membrane upon exocytosis visualized by polarized TIRFM. J Cell Biol 188, 415–428.

Arvan P, Halban PA (2004). Sorting ourselves out: seeking consensus on trafficking in the beta-cell. Traffic 5, 53–61.

Asensio CS, Sirkis DW, Edwards RH (2010). RNAi screen identifies a role for adaptor protein AP-3 in sorting to the regulated secretory pathway. J Cell Biol 191, 1173–1187.

Asensio CS, Sirkis DW, Maas JW Jr, Egami K, To TL, Brodsky FM, Shu X, Cheng Y, Edwards RH (2013). Self-assembly of VPS41 promotes sorting required for biogenesis of the regulated secretory pathway. Dev Cell 27, 425–437.

Assady S, Maor G, Amit M, Itskovitz-Eldor J, Skorecki KL, Tzukerman M (2001). Insulin production by human embryonic stem cells. Diabetes 50, 1691–1697.

Bauer RA (2008). Characterization of Sorting Motifs in the Dense Core Vesicle Membrane Protein Phogrin. Dissertation/PhD Thesis. Ann Arbor, MI: ProQuest Dissertations Publishing.

Blagoveshchenskaya AD, Hewitt EW, Cutler DF (1999). A complex web of signal-dependent trafficking underlies the triorganellar distribution of P-selectin in neuroendocrine PC12 cells. J Cell Biol 145, 1419–1433.

Boncompain G, Divoux S, Gareil N, De Forges H, Lescure A, Latreche L, Mercanti V, Jollivet F, Raposo G, Perez F (2012). Synchronization of secretory protein traffic in populations of cells. Nat Methods 9, 493–498.

Borgonovo B, Ouwendijk J, Solimena M (2006). Biogenesis of secretory granules. Curr Opin Cell Biol 18, 365–370.

Chen Y, Gershlick DC, Park SY, Bonifacino JS (2017). Segregation in the Golgi complex precedes export of endolysosomal proteins in distinct transport carriers. J Cell Biol 216, 4141–4151.

Courel M, Vasquez MS, Hook VY, Mahata SK, Taupenot L (2008). Sorting of the neuroendocrine secretory protein Secretogranin II into the regulated secretory pathway: role of N- and C-terminal alpha-helical domains. J Biol Chem 283, 11807–11822.

Dittie AS, Hajibagheri N, Tooze SA (1996). The AP-1 adaptor complex binds to immature secretory granules from PC12 cells, and is regulated by ADP-ribosylation factor. J Cell Biol 132, 523–536.

Dittie AS, Thomas L, Thomas G, Tooze SA (1997). Interaction of furin in immature secretory granules from neuroendocrine cells with the AP-1 adaptor complex is modulated by casein kinase II phosphorylation. EMBO J 16, 4859–4870.

El Meskini R, Galano GJ, Marx R, Mains RE, Eipper BA (2001). Targeting of membrane proteins to the regulated secretory pathway in anterior pituitary endocrine cells. J Biol Chem 276, 3384–3393.

Emperador-Melero J, Huson V, Van Weering J, Bollmann C, Fischer Von Mollard G, Toonen RF, Verhage M (2018). Vti1a/b regulate synaptic vesicle and dense core vesicle secretion via protein sorting at the Golgi. Nat Commun 9, 3421.

Gandasi NR, Vesto K, Helou M, Yin P, Saras J, Barg S (2015). Survey of red fluorescence proteins as markers for secretory granule exocytosis. PLoS One 10, e0127801.

Hou JC, Min L, Pessin JE (2009). Insulin granule biogenesis, trafficking and exocytosis. Vitam Horm 80, 473–506.

Hummer BH, De Leeuw NF, Burns C, Chen L, Joens MS, Hosford B, Fitzpatrick JJ, Asensio CS (2017). HID-1 controls formation of large dense core vesicles by influencing cargo sorting and trans-Golgi network acidification. Mol Biol Cell 28, 3870–3880.

Jones SM, Howell KE, Henley JR, Cao H, Mcniven MA (1998). Role of dynamin in the formation of transport vesicles from the trans-Golgi network. Science 279, 573–577.

Kockx M, Karunakaran D, Traini M, Xue J, Huang KY, Nawara D, Gaus K, Jessup W, Robinson PJ, Kritharides L (2014). Pharmacological inhibition of dynamin II reduces constitutive protein secretion from primary human macrophages. PLoS One 9, e111186.

Krantz DE, Waites C, Oorschot V, Liu Y, Wilson RI, Tan PK, Klumperman J, Edwards RH (2000). A phosphorylation site regulates sorting of the vesicular acetylcholine transporter to dense core vesicles. J Cell Biol 149, 379–396.

Li H, Waites CL, Staal RG, Dobryy Y, Park J, Sulzer DL, Edwards RH (2005). Sorting of vesicular monoamine transporter 2 to the regulated secretory pathway confers the somatodendritic exocytosis of monoamines. Neuron 48, 619–633.

Liu Y, Schweitzer ES, Nirenberg MJ, Pickel VM, Evans CJ, Edwards RH (1994). Preferential localization of a vesicular monoamine transporter to dense core vesicles in PC12 cells. J Cell Biol 127, 1419–1433.

Milgram SL, Mains RE, Eipper BA (1996). Identification of routing determinants in the cytosolic domain of a secretory granule-associated integral membrane protein. J Biol Chem 271, 17526–17535.

Oprins A, Rabouille C, Posthuma G, Klumperman J, Geuze HJ, Slot JW (2001). The ER to Golgi interface is the major concentration site of secretory proteins in the exocrine pancreatic cell. Traffic 2, 831–838.

Paquin N, Murata Y, Froehlich A, Omura DT, Ailion M, Pender CL, Constantine-Paton M, Horvitz HR (2016). The conserved VPS-50 protein functions in dense-core vesicle maturation and acidification and controls animal behavior. Curr Biol 26, 862–871.

Park JJ, Koshimizu H, Loh YP (2009). Biogenesis and transport of secretory granules to release site in neuroendocrine cells. J Mol Neurosci 37, 151–159.

Rivas RJ, Moore HP (1989). Spatial segregation of the regulated and constitutive secretory pathways. J Cell Biol 109, 51–60.

Sasidharan N, Sumakovic M, Hannemann M, Hegermann J, Liewald JF, Olendrowitz C, Koenig S, Grant BD, Rizzoli SO, Gottschalk A, Eimer S (2012). RAB-5 and RAB-10 cooperate to regulate neuropeptide release in Caenorhabditis elegans. Proc Natl Acad Sci USA 109, 18944–18949.

Sirkis DW, Edwards RH, Asensio CS (2013). Widespread dysregulation of peptide hormone release in mice lacking adaptor protein AP-3. PLoS Genet 9, e1003812.

Suckale J, Solimena M (2010). The insulin secretory granule as a signaling hub. Trends Endocrinol Metab 21, 599–609.

Taraska JW, Perrais D, Ohara-Imaizumi M, Nagamatsu S, Almers W (2003). Secretory granules are recaptured largely intact after stimulated exocytosis in cultured endocrine cells. Proc Natl Acad Sci USA 100, 2070–2075.

Tooze SA (1998). Biogenesis of secretory granules in the trans-Golgi network of neuroendocrine and endocrine cells. Biochim Biophys Acta 1404, 231–244.

Tooze SA, Huttner WB (1990). Cell-free protein sorting to the regulated and constitutive secretory pathways. Cell 60, 837–847.

Topalidou I, Cattin-Ortola J, Pappas AL, Cooper K, Merrihew GE, Maccoss MJ, Ailion M (2016). The EARP complex and its interactor EIPR-1 are required for cargo sorting to dense-core vesicles. PLoS Genet 12, e1006074.

Torii S, Saito N, Kawano A, Zhao S, Izumi T, Takeuchi T (2005). Cytoplasmic transport signal is involved in phogrin targeting and localization to secretory granules. Traffic 6, 1213–1224.

Tsuboi T, Zhao C, Terakawa S, Rutter GA (2000). Simultaneous evanescent wave imaging of insulin vesicle membrane and cargo during a single exocytotic event. Curr Biol 10, 1307–1310.

Vo YP, Hutton JC, Angleson JK (2004). Recycling of the dense-core vesicle membrane protein phogrin in Min6 beta-cells. Biochem Biophys Res Commun 324, 1004–1010.

Weihe E, Schafer MK, Erickson JD, Eiden LE (1994). Localization of vesicular monoamine transporter isoforms (VMAT1 and VMAT2) to endocrine cells and neurons in rat. J Mol Neurosci 5, 149–164.

Zhang X, Jiang S, Mitok KA, Li L, Attie AD, Martin TFJ (2017). BAIAP3, a C2 domain-containing Munc13 protein, controls the fate of dense-core vesicles in neuroendocrine cells. J Cell Biol 216, 2151–2166.